# NOTICE CONCERNING COPYRIGHT RESTRICTIONS

# Imaging Structure with Fluid Fluxes at the Bradys Geothermal Field with Satellite Interferometric Radar (InSAR): New Insights into Reservoir Extent and Structural Controls

**Gary Oppliger[1], Mark Coolbaugh[2] and William Foxall[3]**

**[1]Arthur Brant Laboratory for Exploration Geophysics, UNR**
**[2]Great Basin Center for Geothermal Energy, UNR**
**[3]Lawrence Livermore National Laboratory**

***Keywords***

*Exploration, reservoir characterization, InSAR, interferometry, radar, micro-subsidence, ground-water hydrology*

## ABSTRACT

We present a new example of Interferometric Synthetic Aperture Radar's (InSAR) remarkable utility for defining an operating geothermal reservoir's lateral extent and hydrologically active fracture systems. InSAR reveals millimeter-level surface change due to volume change in the reservoir and overlying aquifer systems caused by fluid pressure reduction and to a lesser extent temperature decrease. Fluid reinjection is revealed in the reverse process as surface inflation. The relevant characteristics and limitations of the InSAR method are discussed. We conclude that when integrated with other geophysical observations and reservoir production data, InSAR analysis will be able to guide new exploration and aid field management.

## Introduction

We report here on the feasibility of using InSAR for understanding controls on hydrologic flow in geothermal reservoirs producing power in the middle capacity range of about 20MW. The Bradys Geothermal field was selected for this study because it is typical of many mid-capacity geothermal fields and has been the subject of several significant geologic investigations (Faulds, 2003) that help place the results in context. The results discussed here are preliminary but clearly demonstrate the practicality of the approach.

For most geothermal fields, incomplete knowledge of reservoir boundaries adds to the risk of new development and exploration work. Commonly, ground-water-level and pressure data are insufficient to delineate the complete geothermal field. In this context, ground deformations mapped with InSAR provide valuable new information on the extent of the reservoir system beyond the known field and possibly on the effectiveness of reinjection wells.

In a geothermal field, surface deformation will occur as a consequence of the production of geothermal fluids even if the reservoir is deep and isolated from shallow groundwater (Vasco, 2002). Reservoir deformation is largely driven by pressure reduction, which reduces the reservoir's compressive strength and allows subsidence of overlying strata into the reservoir; but other factors contribute - including contraction by cooling and possibly viscous drag from fluid flow. Where coupling into a shallow groundwater aquifer occurs, the surface deformation response will contain additional elements (Poland, 1984). These include strain from the newly added weight of deposits that have lost buoyant support, and the simple dehydration shrinkage of clayey deposits. Because all of the above effects are typically associated with production and are centered on the most favored fluid flow axis they are not easily separable. Use of additional data such as groundwater levels and reservoir modeling may help determine their relative significance in a particular case.

Introduced only twelve years ago as a research method with the launch of the European Space Agency's (ESA) ERS 1 satellite, repeat-orbit differential InSAR (InSAR for short) has been showcased for its ability to image earth surface deformation related to earthquakes and volcanic intrusions and more recently ground deformation related to groundwater use, geothermal and petroleum production (Massonnet, 1998). InSAR is a surface displacement change detection method with unprecedented millimeter level sensitivity. Surface displacements that occur in the time interval between the acquisitions of two radar scenes are inferred by comparing the travel times of the radar waves. This is accomplished through combining the two radar scenes to form an interferogram or phase interference image. The anomalous phase patterns represent travel time delay features that technically include contributions from changes in surface displacement, surface moisture and atmospheric moisture. InSAR offers two distinct advantages over traditional optical leveling and GPS for vertical surface change detection. First it can provide map-like images at resolutions of 20-40 meters covering 100 km by 100 km regions. Second, it can be applied in retrospective change studies by using the 12 year archive of ERS 1/2 scenes.

InSAR's ability to monitor surface deformation at geothermal fields has been established on some of the largest fields, e.g. Coso (Fialko, 2000) and models for inversion of reservoir volume strain have been developed and applied (Vasco, 2002). Here we examine the InSAR response over a mid-capacity geothermal field with the intent of demonstrating its effectiveness for revealing subsurface structure relevant to exploration. Notably in this paper, we take the point of view of the resource explorationist rather than the reservoir or geological engineer. This allows interpretation of the data for structural patterns even when the data are too noisy for quantitative assessment of ground displacements. Where quantitative interpretation is important, data decorrelation (noise) masks must be applied to each interferogram. This increases data reliability but suppresses (blanks out) information in large areas.

## Interferogram Formation

With reference to the ESA's ERS 1/2 radar satellites and Jet Propulsion Laboratory's (JPL) Repeat Orbit Interferometry (ROI PAC) processing software, we outline the essential processing steps and data considerations.

### *Radar Scene Acquisition and Focusing*

The ERS 1/2 satellite illuminates the earth to the side of the satellite track with frequency modulated 5.3 GHz radar chirps repeated at 1.7 kHz. The ~4 km wide radar beam propagates across the terrain in the range direction returning a continuous "echo" stream to the satellite receiver. On the ground, chirp compression and Doppler filtering focus the raw radar return to an image with 20 m by 20 m ground resolution. Each ground resolution cell contains a single complex value representing the sum of the real (R) and imaginary (I) (i.e., in-phase and quadrature) returns from all reflectors in that cell. This focused radar image is referred to as Single Look Complex (SLC) image, represented here as

$$SLC_1(x, y) = (R_1 + iI_1), \text{ where i is } \sqrt{-1}.$$

### *Interferogram Formation*

SLC image pairs are spatially registered to better than 0.1 pixel using correlation algorithms; then the images are multiplied point-wise to produce the complex valued interferogram, INT:

$$INT(x, y) = (R_{12} + iI_{12}) = (R_1 + iI_1)\,(R_2 + iI_2)^*,$$

where $^*$ denotes the complex conjugate operator.

$$PHS(x, y) = \text{atan2}(I_{12}, R_{12}),$$

then defines the interferometric or phase difference between two images.

### *Phase Fringes*

In the special case of a zero baseline (or alternatively zero topography) and no ground deformation, the interferogram phase is theoretically constant across the scene. Local ground deformation in the interferogram period alters the radar travel time and is expressed as a relative phase anomaly over the deformed area. In the general case of a non-zero baseline with topography, a terrain-related phase pattern occurs that is easily predicted and removed using a digital elevation model. Where ground deformation exceeds half the radar wavelength, (2.83 cm) the phase vector wraps around, constraining phase between 0 to 2pi. These 2pi intervals are referred to as phase fringes and are rendered in the figures with one full cycle of the color (gray) pallet. The average 23° radar incidence angle of the ERS 1/2 satellite renders it 2.4 times as sensitive to vertical displacement as to displacement in the best coupled horizontal component. One fringe is produced by either 3.07 cm of vertical or 7.24 cm of orbit-track-perpendicular horizontal ground displacement.

## Interferogram Signal and Noise

### *Selecting SLC Image Pairs*

Baseline and time separation are primary interferogram parameters. Preferred scene pairs have no more than 300 meters offset (or perpendicular baseline) in their orbital paths perpendicular to the radar line-of-sight (LOS) vector. The time separation between scenes must be long enough to allow the surface deformation patterns to be well expressed in the interferogram, but not so long that heavy vegetation growth or other surface processes cause a loss of phase correlation between the images.

### *Decorrelation and Noise*

In high rain-fall temperate and tropical regions, vegetation growth drives decorrelation and sets the maximum effective interferogram time interval. In our study area in the Great Basin, sage and scrub growth over five years has little effect. However, we find that areas with wind blown sand or playas are subject to relatively rapid decorrelation. A grid representing surface reflector decorrelation is computed for each interferogram and is available for data quality screening. However, as explained previously, data quality masks are not applied to interferograms shown in the figures as it also interferes with pattern visualization. Areas of high noise in the figures are easily identified as speckled intensity patterns and should be considered highly unreliable. The interferograms in Figures 2 and 3 have been filtered to reduce this short-wavelength noise decorrelation noise. This filtering smoothes areas with minor noise but it also reduces some of the originally available spatial detail.

At longer wavelengths, where noise falls within the ground deformation signal band, tropospheric water vapor variation is the dominant concern. It will occasionally produce phase features that mimic a few centimeters of surface deformation, but it can be identified and minimized by the use of multiple interferogram periods.

### *Dynamic Range*

The dynamic range of InSAR's deformation observation is subject to time and spatial constraints. On the minimum signal

side, our experience has shown that under good atmospheric and ground conditions, surface deformation features with 100 m to 5 km widths and 5 mm displacement over five years can be reliably imaged in a single interferogram. Under these favorable conditions, the non-deformation in-band noise is about 1 - 2 mm. Use of multiple interferograms can further reduce this noise level. On the maximum signal side, there is no practical limit on the total observable deformation, as long as the horizontal gradient in surface displacement projected on the radar LOS vector does not exceed one-half wavelength (2.83cm) per ground resolution cell (20 meters) during the interferogram interval. Our experience suggests for geothermal field observations, a range of interferogram time intervals is desirable to observe both long-wavelength, low-amplitude features distal to the field and short-wavelength, high-amplitude detail near production centers.

## Production Deformation Response

### *The Bradys Hot Springs Geothermal Field*

The Bradys geothermal field lies along the northwest structural boundary between the low relief Hot Springs Mountains and Hot Springs Flats basin, about 80 km east-northeast of Reno, Nevada (Benoit, 1982; Faulds, 2003). The fault-controlled reservoir is developed in permeable zones in Tertiary volcanic rocks in the hanging wall of the Bradys fault, a steeply dipping, north-northeast-striking fault with down-to the-northwest normal displacement. Near the Bradys fault system, Mesozoic metasedimentary basement is overlain by 800 meters or more of Tertiary volcanic and sedimentary rocks. Basement structure and relief is suggested by surface gravity data (Figure 1), (Faulds 2003). The Brady 21-MW dual-flash geothermal plant produces from three clusters of production wells (distributed over ~1.4 km) with an average depth of 930 meters and average fluid temperature of ~156°C. The plant has three clusters of injection wells (spaced over 7 km) with an average injection fluid temperature of ~114°C. (Hess, 2001).

The two presented interferograms, A and B in Figures 2 and 3, respectively cover 2.96 years (92-11-26 to 95-11-04) and 4.78 years (95-11-04 to 00-09-24), They reveal the first micro-subsidence feature reported for the Brady geothermal field. The apparent lack of surface subsidence indications at the field and the feature's low amplitude and broad dimensions may account for it remaining completely unknown until this study. Although our preliminary qualitative analysis here includes only publicly available production data and two interferograms, we hope it is possible for the reader to envision how the use of additional interferograms intervals and detailed production records could produce proportionally more detailed and useful results. As with all preliminary geophysical exploration data, high caution is advised in using interpretations from these two

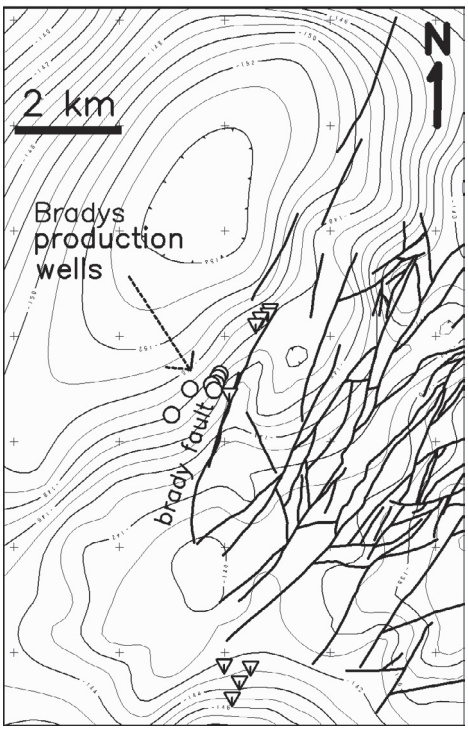


**Figure 1.** Complete bouguer gravity with 1 milligal contours (gray lines) reflects structure and depth to Mesozoic basement. Production wells: circles. Injection wells: triangles. Geologic surface faults: heavy black lines from Benoit, 1982, and Churchill County, Nevada geologic maps.

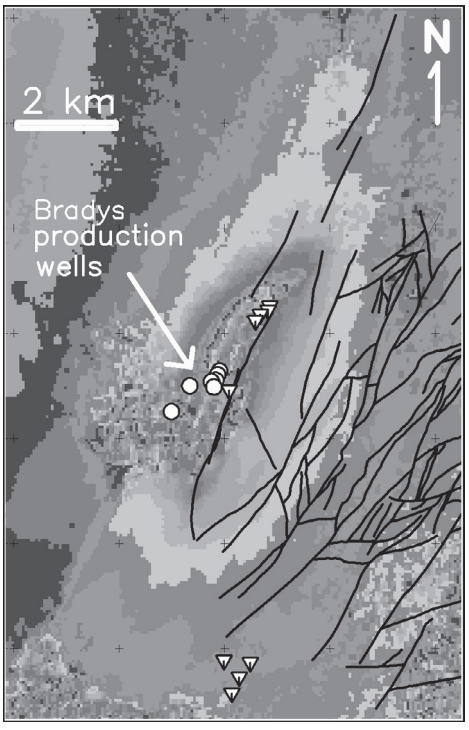


**Figure 2.** Interferogram A - 2.96 years: 92-11-26 to 95-11-04. Each gray intensity change represents 0.16 cm line-of-sight LOS distance change. 18 intensity changes equal one fringe cycle or 2.83 cm LOS or 3.07 cm vertical. Surface faults: heavy black lines. Symbols: see Figure 1.

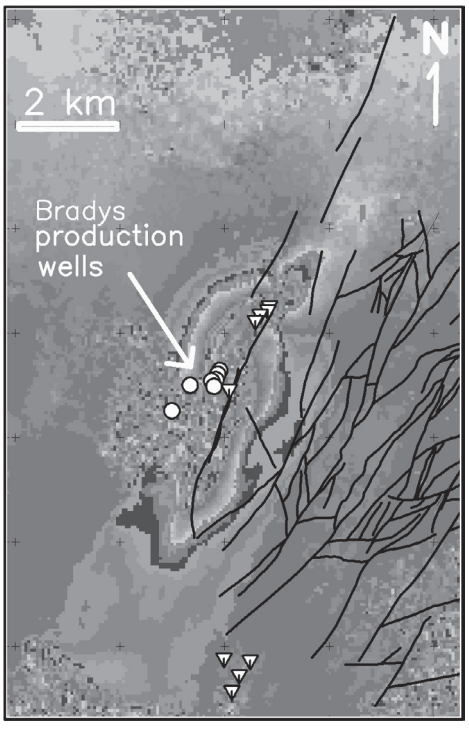


**Figure 3.** Interferogram B - 4.78 years: 95-11-04 to 00-09-24. Each gray intensity change represents 0.16 cm line-of-sight LOS distance change. 18 intensity changes equal one fringe cycle or 2.83 cm LOS or 3.07 cm vertical. Surface faults: heavy black lines. Symbols: see Figure 1.

interferograms to reach hard conclusions about any aspect of the Brady's geothermal field.

At the largest scale, the interferogram phase feature indicates that the production zone has an inner strong hydrologic conductivity zone along a 7 km axis with an outer weaker but seemingly identifiable depression zone for ~11 km total. This is about 6 km more strike length than the field's surface manifestations (fumaroles and sinter). It is remarkable that although production is restricted to a span of less than 2 km, InSAR images may be detecting very subtle signatures several kilometers away. If the interferograms' suggestion of extended reservoir strike length can be verified, the implications for future field development and improved reinjection are potentially significant.

Maximum negative surface flexure in the production area appears to be about 1.3 cm/year. Along northwest profiles, negative surface flexure is centered on the NNE trending Brady fault system and has an inverted bell-form with a ~1.2 km half-width and well defined asymptotes over 4 km on either side. Over the two interferogram periods A and B (Figures 2, 3) the negative surface flexure pattern grows asymmetrically toward the south-southeast, possibly reflecting evolving natural reservoir development. Separate elliptical lobes appear to develop during the second interferogram period on either side of an injection well suggesting a recharge rebound effect. Both interferogram patterns show a split in the deformation pattern north of the known reservoir. One branch continues on a NNE strike, the other branch trends to the NE. These are described further below.

Changing reinjection patterns appear to illuminate an individual hydrologically permeable structure in Interferogram B (Figure 3). Here a strong asymmetric positive flexure (inflation) feature, 1 km wide and 3 km long, appears just northeast of the northern cluster of injection wells. This injection feature is confined to the structural zone delineated by the negative flexure pattern in the previous interferogram interval (Figure 2). The southern boundary of the inflation feature terminates abruptly within the main deflation feature, 300 meters north of the injection well.

## Conclusions

InSAR is just beginning to reveal its potential to trace and characterize the hydrologically active fracture systems in geothermal reserviors. When integrated and validated with other geophysical observation and reservoir production information, such analysis should be able to guide new exploration wells and improve field management by improving reinjection patterns. We note that the cost of a multiple interferogram InSAR geothermal field study is comparable to an aeromagnetic or ground gravity survey.

## Acknowledgements

This work was supported by the Department of Energy under DE-FG36-02ID14311 through the Great Basin Center for Geothermal Energy. Additional support was provided by the Arthur Brant Laboratory for Exploration Geophysics, University of Nevada Reno. We would like to thank both Ormat International Inc. for access to the study area, and their staff for helpful discussions. The European Space Agency ERS 1/2 raw SAR scenes were provided through the Western North American InSAR (WInSAR) research consortium and JPL's ROI_PAC Research Interferometry package version 2.2.2 was used to prepare the interferograms.

## References

Benoit, W.R., Hiner, J.E., and Forest, R.T., 1982, Discovery and geology of the Desert Peak geothermal field: A case history: Nevada Bureau of Mines and Geology Bulletin 97, 82 p.

Faulds, J., Garside, L., Oppliger, G., 2003, Structural Analysis of the Desert Peak-Brady Geothermal Fields, Northwestern Nevada, Geothermal Resources Council Transactions v. 27, p. 859-864.

Fialko, Y., and M. Simons, 2000, Deformation and seismicity in the Coso geothermal area, Inyo County, California: Observations and modeling using satellite radar interferometry, Journal of Geophysical Research, v. 105, p. 21,781-21,794.

Hess, R., 2002, Geothermal Energy in Nevada Bureau of Mines and Geology SP MI-2001 The Nevada Mineral Industry 2002.

Massonnet, D. and Feigl, K. L., 1998, Radar interferometry and its application to changes in the earth's surface, Reviews of Geophysics, v. 36(4), p. 441-500.

Poland, J.F., 1984, Mechanics of land subsidence due to fluid withdrawal, in Poland, J.F., editor, Guidebook to studies of land subsidence due to ground-water withdrawal: Studies and Reports in Hydrology 40, UNESCO, p. 37-54.

Vasco, D.W., Wicks, C., Jr. , and Karasaki, K., 2002, Geodetic imaging: High-resolution reservoir monitoring using satellite interferometry, Geophysical Journal International, v. 149, p. 555-571.